Photochemical modeling of the southern California Air Quality Study

ARTICLE *in* ENVIRONMENTAL SCIENCE AND TECHNOLOGY · FEBRUARY 1993

Impact Factor: 5.33 · DOI: 10.1021/es00039a019

5 AUTHORS, INCLUDING:

Robert A Harley
University of California, Berkeley
150 PUBLICATIONS **5,600** CITATIONS
SEE PROFILE

Armistead G Russell
Georgia Institute of Technology
285 PUBLICATIONS **6,112** CITATIONS
SEE PROFILE

Environ. Sci. Technol. 1993, 27, 378-388

Photochemical Modeling of the Southern California Air Quality Study

Robert A. Harley,[†] Armistead G. Russell,[‡] Gregory J. McRae,[‡,§] Glen R. Cass,[*,†] and John H. Seinfeld[†]

Engineering and Public Policy Department, Carnegie Mellon University, Pittsburgh, Pennsylvania 15213, and Environmental Quality Laboratory, California Institute of Technology, Pasadena, California 91125

■ The Southern California Air Quality Study (SCAQS) provides detailed experimental observations that can be used to explore the causes of the Los Angeles smog problem. In the present study, the CIT photochemical airshed model is updated and then applied to the August 27–29, 1987, SCAQS intensive monitoring period. Using measured meteorological parameters, measured initial and boundary conditions, and the official emission inventory prepared by the government, ozone concentrations are underpredicted by 23% on average. Recent field experiments suggest that emissions of organic gases and carbon monoxide are understated in the official emission inventory. When the organic gas emissions from on-road vehicle engine exhaust are increased as suggested by emission rate measurements made in a Los Angeles area roadway tunnel during SCAQS, ozone predictions match the observed concentrations more closely (the mean normalized bias in ozone predictions for this case is +1%). Reactive hydrocarbon concentrations are underpredicted by 35% in the base case calculation, but are underpredicted by only 12% in the increased emission case. Results of this study thus support prior estimates that the organic gas emissions in Los Angeles have been understated in recent years.

1. Introduction

Concentrations of ozone in the boundary layer of urban and rural atmospheres continue to exceed standards designed to protect human health, despite more than 25 years of effort and billions of dollars of investment in technology to control emissions of ozone precursors (*1*). Mathematical models have been developed that describe the formation and transport of ozone and other components of photochemical smog based on knowledge of atmospheric chemistry, meteorology, and pollutant emissions to the atmosphere (*1*, *2*). In this paper we describe improvements to an existing Eulerian photochemical air quality model (*3–5*), referred to as the CIT airshed model. Earlier versions of this model have been used to study photochemical smog formation in the Los Angeles area (*4*, *5*), formation and control of nitrogen-containing pollutants (*5*, *6*), spatial patterns in pollutant responses to emission controls (*7*), effect of methanol fuel use in motor vehicles (*8*), and modeling and control of deposition of nitrogen-containing air pollutants (*9*).

This paper describes the application of the CIT airshed model to the August 27–29, 1987, period in the Los Angeles, CA, area. This 3-day interval was one of the intensive monitoring periods of the Southern California Air Quality Study (SCAQS; for an overview, see ref 10), which took place during the summer and fall of 1987. As part of SCAQS, a variety of special meteorological and air quality measurements were carried out to supplement the routine measurements made in the Los Angeles area, thus providing a very detailed ambient data set expressly designed for supporting and testing photochemical airshed models. Data collected during SCAQS will form the basis for many air pollution control decisions in the Los Angeles area over the next decade. In addition, the decisions made in Los Angeles will influence air pollution control policies elsewhere. Several recent studies have questioned the accuracy of the official emission inventory for organic gases and carbon monoxide in the Los Angeles area (*1*, *11–13*). If the emissions of organic gases are in fact understated in the official inventory, the air pollution control problem in Los Angeles may be more difficult than was previously thought. It is therefore important that the relationship between emissions and ambient air quality be explored thoroughly for the SCAQS experiment.

In the course of the present study, revisions to the CIT photochemical airshed model have been made. In particular, an extended version of the chemical mechanism of Lurmann et al. (*14*) and an improved dry deposition module (*9*) have been incorporated into the model. Further changes have been made to allow for representation of the observed spatial variations in the total and ultraviolet component of the solar radiation flux. These changes are described in greater detail later in the text.

2. Model Description

Photochemical models such as the CIT airshed model are based on numerical solution of the atmospheric diffusion equation, which is written repeatedly for each chemical species of interest:

$$\frac{\partial C_i}{\partial t} + \nabla\cdot(\vec{u}C_i) = \nabla\cdot(\mathbf{K}\nabla C_i) + R_i + Q_i \qquad (1)$$

where C_i is the ensemble mean concentration of species i, $\vec{u}$ is the mean wind velocity, $\mathbf{K}$ is the eddy diffusivity tensor (here assumed to be diagonal), R_i is the rate of generation of species i by chemical reactions, and Q_i is a source term for elevated point sources of species i. Boundary and initial conditions, along with meteorological data and emission fields, complete the specification of the problem. The surface boundary condition sets the upward flux of each pollutant to be equal to direct emissions minus the dry deposition flux:

$$-K_{zz}\frac{\partial C_i}{\partial z} = E_i - v_g^i C_i \qquad (2)$$

where K_{zz} is the vertical eddy diffusivity, E_i is the ground-level emission flux, and v_g^i is the dry deposition velocity for species i. A no-flux boundary condition is applied at the top of the modeling region. Lateral boundary conditions and initial conditions throughout the modeling region are established using measured pollutant concentration data.

The details of the mathematical model and numerical solution techniques that are used in this study have been described previously (*3*, *5*, *15*). A number of improvements have been made to an earlier version of this model (*5*), as described in the following sections. A detailed description of the model, recent enhancements, and performance evaluation is also presented in ref 15. A three-volume user's manual for the CIT airshed model has been prepared. These volumes describe installation and operation of the model (*16*), data preparation and formats (*17*), and

[†] California Institute of Technology.
[‡] Carnegie Mellon University.
[§] Present address: Chemical Engineering Department, Massachusetts Institute of Technology, Cambridge, MA 02139.

 0013-936X/93/0927-0378$04.00/0

Table I. Complete List of Species Defined in the Chemical Mechanism

species code	species name	species code	species name
	Differential Species		
NO	nitric oxide	MGLY	methyl glyoxal
NO_2	nitrogen dioxide	PAN	peroxyacetyl nitrate
O_3	ozone	RO_2	total RO_2 radicals
HONO	nitrous acid	MCO_3	CH_3CO_3 radical
HNO_3	nitric acid	ALKN	alkyl nitrate
HNO_4	pernitric acid	ALKA	C_4+ alkanes[a,b]
N_2O_5	dinitrogen pentaoxide	ETHE	ethene
NO_3	nitrogen trioxide	ALKE	C_3+ alkenes
HO_2	hydroperoxy radical	TOLU	toluene
CO	carbon monoxide	AROM	higher aromatics
HCHO	formaldehyde	DIAL	unknown dicarbonyls
ALD2	acetaldehyde	CRES	cresol
MEK	methyl ethyl ketone	NPHE	nitrophenols
	Steady-State Species		
OSD	oxygen singlet D	RO_2N	alkyl nitrate RO_2
O	atomic oxygen	RO_2P	phenol RO_2
OH	hydroxyl radical	BZN_2	benzaldehyde N-RO_2
RO_2R	general RO_2 1	BZO	phenoxy radical
R_2O_2	general RO_2 2		
	Newly Added Species[c]		
H_2O_2	hydrogen peroxide	NH_3	ammonia
MeOH	methanol	NIT	aerosol nitrate
EtOH	ethanol	SO_2	sulfur dioxide
MTBE	methyl *tert*-butyl ether	SO_3	sulfur trioxide
		CH_4	methane
ISOP	isoprene		

[a] 50% of propane emissions also assigned to the lumped alkane class; remaining propane emissions treated as unreactive, as per Lurmann et al. (*14*). [b] 30% of benzene emissions also assigned to the lumped alkane class, as per Lurmann et al. (*14*). [c] This study.

the computer source code (*18*).

2.1. Chemical Mechanism. The condensed version of the LCC chemical mechanism (Lurmann, Carter, and Coyner, ref 14) has been incorporated into the CIT airshed model. The published mechanism includes 26 differential and 9 steady-state chemical species.

In addition to the eight lumped organic classes specified by Lurmann et al. (*14*), the chemical mechanism has been expanded to include, explicitly, the chemistry of methane, methanol, ethanol, methyl *tert*-butyl ether (MTBE), isoprene, hydrogen peroxide, and sulfur dioxide. The complete list of chemical species defined in the extended chemical mechanism is shown in Table I. All of the reactions beyond those listed in the published version of the LCC mechanism are shown in Table II. Methane is not followed dynamically in the model, but instead a constant background concentration of 2.2 ppm is applied. Isoprene is used as a surrogate for all biogenic hydrocarbon emissions in the present model. The oxygenated species (methanol, ethanol, and MTBE) are of interest as ingredients in alternative or reformulated motor vehicle fuels (*8*). The introduction of reformulated motor vehicle fuels containing MTBE did not occur in the Los Angeles area until after the 1987 SCAQS experiment, so therefore there are no emissions of MTBE for the calculations described in the present study.

2.2. Dry Deposition. Because dry deposition fluxes influence atmospheric pollutant concentrations and may adversely affect vegetation and building materials, air quality models should include a thorough calculation of dry deposition velocities. Earlier versions of the CIT airshed model (*3*, *5*) calculated a fluid-mechanically determined upper limit value for the dry deposition velocity based on local surface roughness and meteorological conditions and then applied species-specific linear attenuation factors to estimate the actual deposition velocities for species that are removed by dry deposition at less than the diffusion-limited rate.

A new dry deposition scheme described by Russell et al. (*9*) has been incorporated into the present version of the model. As before (*3*), a maximum deposition velocity ($v_{g\,max}$) is calculated for each grid square by assuming that the surface acts as a perfect sink for the depositing pollutant:

$$v_{g\,max} = \frac{k^2 u(z_r)}{\left[\int_{z_0}^{z_r} \phi_m\left(\frac{z}{L}\right)\frac{dz}{z}\right]\left[2\left(\frac{Sc}{Pr}\right)^{2/3} + \int_{z_0}^{z_r} \phi_p\left(\frac{z}{L}\right)\frac{dz}{z}\right]} \quad (3)$$

where k is von Karman's constant, $u(z_r)$ is the wind speed at the reference elevation z_r, z_0 is the surface roughness length, L is the Monin–Obukhov length, Sc is the Schmidt number, and Pr is the Prandtl number. The functions ϕ_m and ϕ_p are based on the momentum and heat flux-profile relationships of Businger et al. (*24*).

The dry deposition velocity v_g^i for each species is calculated as a function of $v_{g\,max}$ and a surface resistance term that depends on the surface type (i.e., land use) and the solar radiation flux:

$$v_g^i = \frac{1}{(1/v_{g\,max}) + r_s^i} \quad (4)$$

where r_s^i is the surface resistance term for chemical species

Table II. Chemical Reactions Added to LCC Mechanism

reactn no.	chemical reaction	rate const[a]	ref
96	$H_2O_2 + h\nu \rightarrow 2OH$	[b]	14
97	$H_2O_2 + OH \rightarrow HO_2 + H_2O$	$1.36 \times 10^6/Te^{-187/T}$	14
98	$MeOH + OH \rightarrow HCHO + HO_2$	$2.81Te^{148/T}$	19
99	$CH_4 + OH \rightarrow HCHO + RO_2 + RO_2R$	$3.06Te^{-1282/T}$	19
100	$ISOP + OH \rightarrow HCHO + ALD2 + RO_2 + RO_2R$	$1.12 \times 10^7/Te^{410/T}$	19
101	$ISOP + O_3 \rightarrow 0.5HCHO + 0.65ALD2 + 0.21MEK + 0.16HO_2 + 0.29CO + 0.06OH + 0.14\ RO_2 + 0.14\ RO_2R$	$5.41 \times 10^3/Te^{-2013/T}$	19
102	$ISOP + O \rightarrow 0.4HO_2 + 0.5MEK + 0.5ALD2$	$2.64 \times 10^7/T$	19
103	$ISOP + NO_3 \rightarrow NO_2 + HCHO + ALD2 + RO_2 + R_2O_2$	$1.12 \times 10^7/Te^{-1121/T}$	19
104	$EtOH + OH \rightarrow ALD2 + HO_2$	$2.72Te^{532/T}$	19
105	$MTBE + 1.4OH^c \rightarrow 0.4HCHO + 0.4MEK + 1.8RO_2 + 1.4RO_2R + 0.4R_2O_2 + 0.6TBF^d$	$3.00Te^{460/T}$	20, 21
106	$SO_2 + OH \rightarrow SO_3 + HO_2$	$4.00 \times 10^5/T$	19[e]
107	$HNO_3 + NH_3 \leftrightarrow NIT$	[f]	22, 23

[a] In units of $ppm^{-1}\ min^{-1}$, with T specified in degrees kelvin. [b] Photolysis rate constant (min^{-1}) depends on light intensity. [c] The rate expression is simply k[MTBE][OH]. Additional hydroxyl radicals are consumed because an intermediate product is assumed to be oxidized rapidly. [d] *tert*-Butyl formate (TBF) is treated as an inert species. [e] Approximate expression obtained by assuming p = 1 atm. [f] Ammonium nitrate aerosol (NIT) is assumed to exist in equilibrium with gas-phase nitric acid and ammonia.

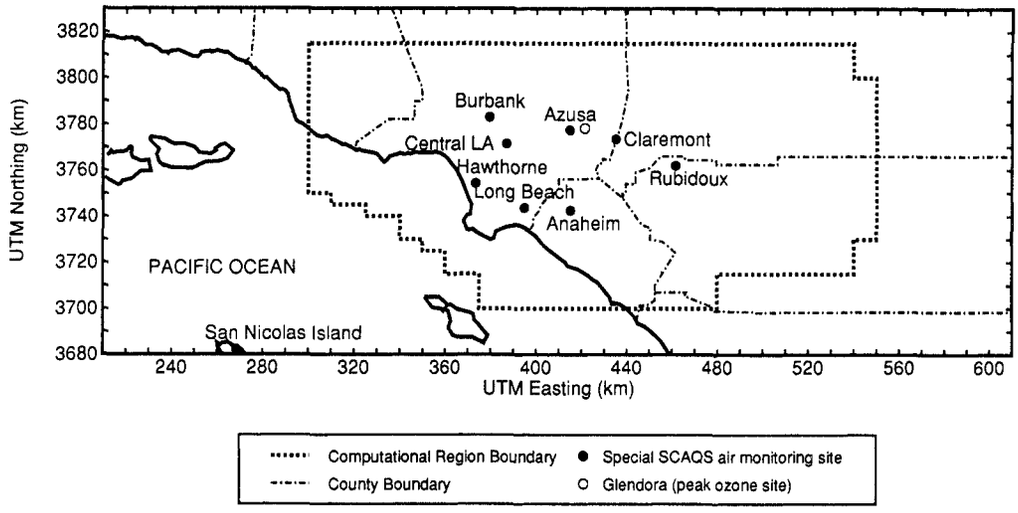

Figure 1. Map of the Los Angeles, CA, area showing the computational region and the locations of special SCAQS air quality monitoring sites.

i. Separate values of r_s^i are specified for each chemical species and each of 32 land-use types, based on the advice of Sheih et al. (*25*) and engineering judgement (*9*).

2.3. Solar Radiation Fields. Rate constants for photolysis reactions are usually estimated using a model that predicts the actinic flux at various wavelengths given the solar zenith angle (*26*), and from published values of the absorption cross sections and quantum yields for those species that undergo photolysis. The actual photolysis rates may differ from predicted values due to seasonal and local variations in pollutant concentrations and cloud cover. There can also be a pronounced increase in radiation intensity in the vertical direction above ground level (*26*).

Solar radiometers are available that measure the broadband ultraviolet component (295–385 nm) of the incoming radiation. Data from such instruments can be used to estimate directly the NO_2 photolysis rate (*27, 28*). This issue will be discussed later in the text with reference to SCAQS.

The CIT airshed model has been modified to accept a spatially and temporally resolved ground-level photolysis scaling factor field, plus a single regionwide correction factor that can be applied at the upper boundary of the modeling region. Linear interpolation of the photolysis scaling factors between ground level and the top of the modeling region is used to estimate the vertical variation of photolysis rate constants, creating in effect a three-dimensional ultraviolet radiation field.

The total (as opposed to ultraviolet) solar flux can also exhibit significant variations from predictions that assume clear sky conditions. Within the model, the total solar radiation flux is first computed as a function of the solar zenith angle by assuming clear sky conditions (*29*). Then these clear sky solar radiation values are corrected to account for the spatial distribution of cloud cover. Direct measurements of the total radiation flux are the preferable means for computing solar flux scaling factors, but scaling factors can also be estimated based on the fraction of sky covered by clouds using formulas of the form $1 + b_1 N^{b_2}$, where N is the fraction of sky obscured by clouds and b_1 and b_2 are empirical constants (*29*). The CIT airshed model has been further modified to accept a temporally and spatially resolved total solar radiation scaling factor field.

3. *Model Application to August SCAQS*

In this section, the application of the CIT airshed model is described for a 3-day period during summer 1987 in the Los Angeles, CA, area. The particular days selected encompass one of the intensive monitoring periods of SCAQS: the episode being simulated begins on Thursday, August 27 and continues through Saturday, August 29. The highest measured ozone concentration for this period was observed at Glendora on August 28, with a peak 1-h average value of 29 pphm reported.

The geographical region under consideration is shown in Figure 1. For the purposes of the present air quality modeling calculations, a regular 5 by 5 km square grid system was superimposed on the region, and emissions and meteorological data were specified at each grid square as described later in the text. The modeling region extended to a height of 1100 m above ground level, with the vertical dimension subdivided into five computational layers. The thicknesses of these five layers, beginning at ground level, were 38, 116, 154, 363, and 429 m.

3.1. Emission Inventory. Detailed pollutant emission data are required for the application of photochemical models. The emission inventory must be both spatially and temporally resolved. A special emission inventory development program for SCAQS has been undertaken (*30*). This effort resulted in a set of day-specific data files that specify the emissions of carbon monoxide, oxides of nitrogen, total organic gases, oxides of sulfur, and particulate matter at a spatial resolution of 5 km. The temporal resolution is hourly, although in some cases only daily emissions totals are specified, and a source-specific diurnal variation profile is applied to obtain hourly emissions.

The emission inventory used in this study was received from the California Air Resources Board (*31*). Mobile source emission estimates were based on a travel demand model and the EMFAC 7E emission factor model (*32*). Stationary source emission estimates were prepared by the South Coast Air Quality Management District. These estimates include day-specific power plant, aircraft, and refinery emissions. A highly aggregated summary of the emission inventory for August 27 is presented in Table III. The detailed inventory includes emissions from more than 800 source types, with the organic gas emissions broken down into 280 detailed chemical species. The inventory region includes the South Coast Air Basin plus parts of the Southeast Desert Air Basin (to the north and east of the mountains surrounding the Los Angeles area) and parts of Ventura County to the northwest.

The mobile source emission inventories provided for use in this study are all based on identical weekday traffic flow patterns, even though the last day of the modeling period falls on a Saturday. The mobile source inventories are only

Table III. Regionwide[a] Emissions Summary for August 27, 1987

source type	base case emissions (10^3 kg/day) NMOG[b]	NO_x	CO
on-road vehicle gasoline engines			
cold exhaust	150	*c*	*c*
hot exhaust	296	*c*	*c*
evaporative emissions			
running losses	51		
hot soak	98		
diurnal	24		
on-road diesel engine exhaust	26	*c*	*c*
subtotal on-road vehicles	645	678	4743
other mobile sources	61	124	418
stationary source fuel combination	29	259	204
organic solvent emissions			
surface coatings	363		
domestic products	97		
degreasing and cleaning	109		
pesticides	31		
biogenic emissions	117		
all other sources	410	77	259
grand totals	1745	1138	5624

[a] The inventory region covers most of the area shown in Figure 1, which includes portions of the Southeast Desert Air Basin and portions of Ventura County, in addition to the entire South Coast Air Basin. [b] Non-methane organic gases. [c] On-road vehicle NO_x and CO exhaust emissions were not broken down into subcategories in the official inventory.

"day specific" in that they are corrected for spatial and diurnal variations in temperature. Separate stationary source emission estimates for weekdays and weekends were prepared and were used in this study as appropriate. As a sensitivity test, an alternate emission inventory using increased mobile source exhaust emission factors was prepared. This was done in an attempt to explore the higher on-road vehicle emission rates suggested by a recent study of emissions measured within a roadway tunnel in the Los Angeles area (*11*). The on-road vehicle hot exhaust emissions of carbon monoxide and organic gases were increased to 3 times the EMFAC 7E values. Although this exhaust emission increase is substantial for the particular source categories affected, it is not large in the context of the total organic gas emission inventory (before being scaled up, the on-road vehicle hot exhaust emissions represented 17% of the total baseline organic gas emissions from all sources combined, as shown in Table III). There are also uncertainties associated with the estimates for mobile source cold start and evaporative emissions, for stationary source emissions, and for biogenic emissions. However, for the purposes of the present hot exhaust emission sensitivity analysis, emissions from other source categories were not changed.

In addition to the anthropogenic emissions discussed above, there are emissions of isoprene and terpenes from natural and urban vegetation. A study by Winer (*33*) measured organic gas emission factors for many different plant species found in southern California, including various urban ornamental plants. A later study investigated organic gas emissions from crops (*34*). Based on a new gridded inventory of leaf biomass in the Los Angeles area (*35*), and temperature and solar radiation data for August 27 and 28, new day-specific biogenic emission inventories were prepared (*36*). Because no day-specific biogenic inventory for August 29 was available, the biogenic inventory for August 28 was used for both August 28 and 29.

An ammonia emission inventory also is included in these calculations. The inventory used in this study is the 1982 South Coast Air Basin inventory of Gharib and Cass (*37*). The basinwide emissions of ammonia were estimated to be 164 tons/day, with over half of the emissions coming from livestock. A revised ammonia emission inventory is being prepared as part of the SCAQS research effort (*38*), but was not available in time for inclusion in this study.

Organic gas speciation profiles have been assigned to each source type and were used to compute detailed emissions of individual organic species from the total organic gas emissions. Speciation of both organic gas emissions and emissions of NO_x and SO_x was based on data supplied with the official emission inventory (*31*). The detailed organics (resolved to the level of individual chemical species or isomers of a particular compound) were recombined into a smaller number of lumped organic classes. In this study, assignment of individual organic species to lumped organic classes is extended from Lurmann et al. (*14*). In general, compounds with similar chemical properties are lumped together and the chemistry of all compounds assigned to a lumped species group is represented by one or more surrogate species. For example, toluene, ethylbenzene, and other monoalkylbenzenes are lumped together and toluene is used as the surrogate species. The lumping procedure has been revised to account for extensions to the chemical mechanism, so that alcohols are lumped separately from the alkanes, and biogenic alkenes are lumped separately from the other alkenes. Further, the original lumping procedure from Table IV-3 of Lurmann et al. (*14*) does not include the complete list of chemical species referenced in the current emission inventory, so lumping assignments were made for the new species by analogy to assignments for existing species.

3.2. Meteorological Data. The database of routine and special SCAQS measurements was obtained from the California Air Resources Board (*39*). Wind, temperature, humidity, solar radiation, air quality, and upper air sounding data were extracted from this database and processed to provide the input data required by the CIT airshed model. To develop spatially complete fields for use in the present study, data values were estimated for each cell in a regular 5 by 5 km square grid system from measured data at nearby monitoring sites, using a weighted interpolation scheme (*40, 41*). In this scheme, the influence of a monitoring site on interpolated values varies inversely with distance squared between the monitor and the interpolation point. Large topographic features such as mountain ranges are represented by interpolation barriers, so that measured data from stations lying on the far side of a mountain range do not influence interpolated values on the near side.

The interpolation procedures were applied directly to scalar fields such as temperature and humidity. In the case of wind vectors, the interpolation formula was applied separately to the x- and y-components of the wind velocity, and then a smoothing procedure was applied to reduce field divergence (*41*). During the development of hourly surface level wind fields, data from 50 wind stations that were reported in an hourly average form were used. Since the interpolation procedures assume that station measurements represent the wind flow over several adjacent model grid squares, wind stations located in narrow valleys such as Banning Pass and Simi Valley were not used because they are representative of only very local conditions. Special SCAQS wind measurements made on top of hills at Catalina Island, Henninger Flats, Kellogg Hill, and Palos

Verdes were not used in the generation of surface level wind fields because these stations were intended to characterize winds aloft as they impinged on major obstacles to flow.

As part of SCAQS, a greatly expanded upper air measurement program was undertaken on all of the intensive monitoring days (*42*). Upper air soundings were performed six times per day at a network of eight sites covering the coastal and inland regions of the air basin. Additional upper air sounding data were available at several other sites, but the sampling schedule at these sites called for only two to three soundings per day. Data on winds up to 1500 m above ground level were extracted from these rawinsonde and airsonde measurements and were input directly to the objective analysis program to generate three-dimensional wind fields (*41*). These upper air soundings provide information about winds and temperature structure aloft and are especially useful in the inland portions of the air basin where upper air soundings seldom are available.

Mixing heights were inferred from plots of the vertical profile of potential temperature derived from the upper air soundings. Typical daytime soundings during the August 27–29 period exhibited well-defined inversion layers atop neutral and unstable layers near the surface. Nocturnal ground-based inversions for August 27–29 were only observed at the inland sites of Ontario and Riverside. The condition of the nocturnal boundary layer, as indicated by upper air soundings made at other sites, was generally only slightly stable or neutral. Such behavior is expected in urban areas, where buildings and heat island effects disturb the boundary layer and inhibit the development of strong ground-based nocturnal inversions (*43*). For this reason, the CIT airshed model has been modified to enforce a minimum Monin–Obukhov length of 50 m at night. Further, the method for calculating the vertical diffusivity profile under stable conditions in the revised CIT airshed model differs slightly from the method specified by McRae et al. (*3*). The new profile for K_{zz} is

$$K_{zz} = \begin{cases} \dfrac{ku_*z}{0.74 + 4.7(z/L)} & \text{for } z < L \\ K_L & \text{for } L \le z < Z_i \\ 0.05K_L & \text{for } z \ge Z_i \end{cases} \quad (5)$$

where k is Von Karman's constant, u_* is the friction velocity, z is the elevation above ground level, L is the Monon–Obukhov length, Z_i is the height of the base of the lowest strong inversion layer, and K_L is the vertical diffusivity evaluated at $z = L$ using the first expression above. The nighttime atmosphere is assumed to be slightly stable for elevations below the strong inversion base.

Hourly measurements of dry bulb temperature were reported at about 60 sites in the Los Angeles area during the SCAQS experiment. In processing these data, isolated missing hours of data were filled in by linear interpolation. Hourly averaged temperature data were reconciled with short averaging time data by interpolating between short-term data points to obtain estimates of the hourly average temperature. Relative humidity and dew point measurements reported at over 40 sites were converted to absolute water vapor concentrations in parts per million, using a relationship between temperature and the saturation vapor pressure of water (*44*).

Solar ultraviolet radiometers were operated at five locations during the summer phase of SCAQS. Measurements were made at Long Beach, Central Los Angeles, Rubidoux, Claremont, and on top of Mount Wilson, at an elevation of 1741 m above sea level. The radiometer data were used to estimate actual NO_2 photolysis rates, according to the following best-fit relationship:

$$J = [0.16(1 - \cos \chi_0) + 0.088]E \quad (6)$$

where χ_0 is the solar zenith angle, E is the measured solar ultraviolet irradiance (mW/cm^2), and J is the NO_2 photolysis rate constant (min^{-1}). This relationship is based on comparisons of UV radiometer data with simultaneous measurements of the NO_2 photolysis rate (*27*). Recently a more general expression relating J to E has been developed that is consistent with radiative transfer theory (*28*). Use of this expression results in similar values for J.

In previous modeling studies, the clear sky NO_2 photolysis rate constant J^* generally has been estimated using the expression

$$J^* = \int_0^\infty \sigma(\lambda)\varphi(\lambda)F(\lambda,\chi_0,z)\, d\lambda \quad (7)$$

where values of the absorption cross section σ and the quantum yield φ were derived from experimental data and values of the actinic flux F (as a function of wavelength λ, solar zenith angle χ_0, and elevation z) were based on the predictions of a radiative-transfer model (*26*). In the present study, photolysis scaling factors are computed as the ratio of the actual photolysis rate J to the theoretical clear sky value J^* at each station and at each hour where measured irradiance data are available.

Although the photolysis scaling factors computed as described above sometimes show large departures from unity in the early morning and late afternoon hours, photolysis rates at these times are very low. Typical midday values for the UV scaling factor on August 27–29 are 1.0 at Central Los Angeles, 0.8 at Claremont, 0.65 at Rubidoux, 0.4 at Long Beach, and 1.2 at Mount Wilson. These factors indicate that the actual photolysis rates vary considerably from those calculated using the actinic flux estimates of Peterson (*26*).

The Long Beach UV measurements for the entire second half of the summer SCAQS experiment (i.e., August and September) were consistently much lower than values reported at other sites, despite reported clear sky conditions at nearby airports. Because of this discrepancy, the Long Beach measurements were not included when the final UV scaling field was constructed.

3.3. Boundary and Initial Conditions. Boundary and initial conditions are specified using routine surface-level air quality measurements and aircraft-based measurements acquired during SCAQS (*45*), and from data in the report by Main et al. (*46*). Routine hourly concentration measurements are available for ozone, carbon monoxide, nitric oxide, nitrogen dioxide, sulfur dioxide, and non-methane hydrocarbons (NMHC). Ozone concentration measurements are abundant in the Los Angeles area, with over 50 stations routinely reporting hourly average concentrations. Oxides of nitrogen measurements are reported at about 35 stations, whereas routine hydrocarbon concentration measurements are reported at only 12 sites. There is no detailed chemical speciation reported for the routine hydrocarbon measurements, although in some cases measurements of both total hydrocarbon (THC) and methane concentrations are made, thus permitting direct calculation of NMHC concentrations.

Where only total hydrocarbon concentrations were reported, without matching methane data, the NMHC concentrations in parts per million of carbon were estimated as

$$\text{NMHC} = (\text{THC} - 1.7)/1.68 \quad (8)$$

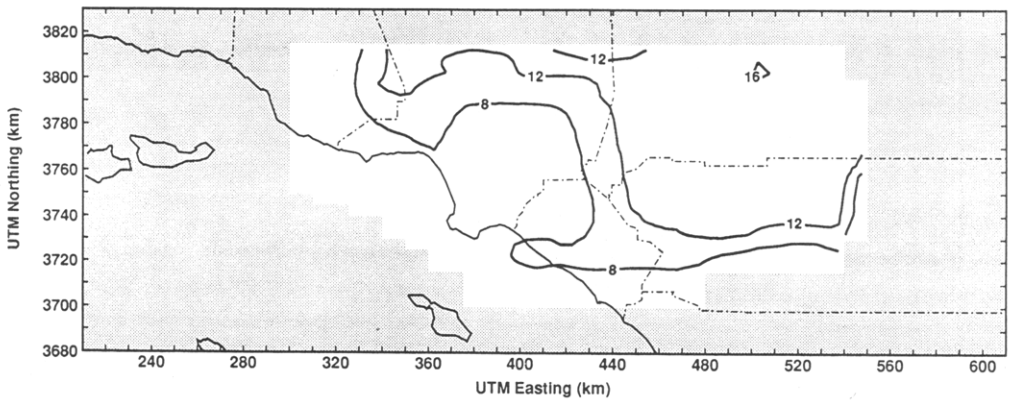

Figure 2. Spatial distribution of ground-level 1-h average ozone concentrations (in parts per hundred million, pphm) at 1400–1500 h PST on August 28, as calculated using the CIT airshed model and the base case emission inventory.

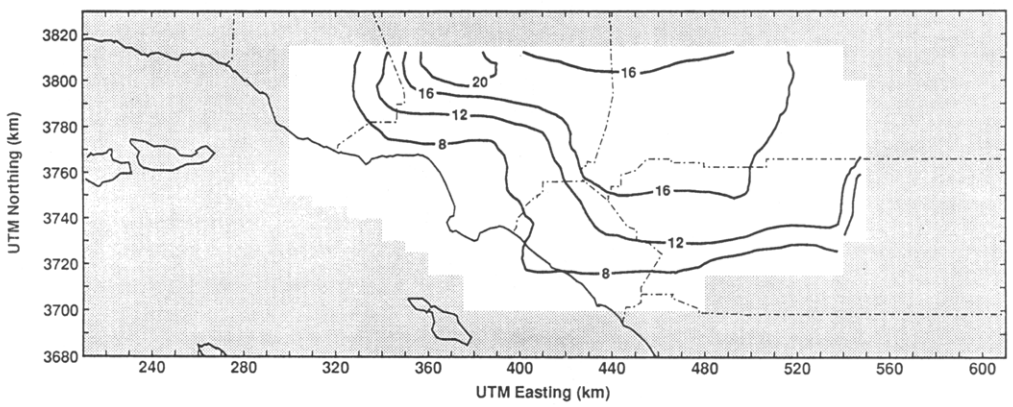

Figure 3. Spatial distribution of ground-level 1-h average ozone concentrations (pphm) at 1400–1500 h PST on August 28, calculated using increased on-road vehicle hot exhaust emissions of organic gases and carbon monoxide.

based on CH_4/NMHC correlations for Los Angeles (*15*). The value 1.7 ppm C is representative of the background methane concentration as measured at San Nicolas Island, and the factor 1.68 accounts for methane emissions within the air basin. The routinely available hydrocarbon concentration measurements specify only THC and sometimes methane, without any further chemical speciation. Therefore, these NMHC concentrations were speciated within the model based on detailed hydrocarbon concentration data measured during SCAQS (*47*), as shown in footnote *c*, Table IV. Within urban areas, aldehyde and ketone boundary and initial conditions were set proportional to NMHC and over the ocean were set using aldehyde and ketone concentrations measured upwind at San Nicolas Island (*46*). Values for the upwind (inflow) boundary conditions used for the base case model simulation are given in Table IV.

Table IV. Upwind[a] Boundary Condition (BC) Values (ppb)

species	base case	increased BC case[b]
CO	200	200
NO_2	1	1
NO	1	1
HCHO	3	24
ALD2	5	5
MEK	4	4
NMHC[c]	100	250
O_3	40	100

[a] Downwind boundary conditions are based on the advection flux out of the air basin. The boundary condition at the top of the modeling region (at a height of 1100 m above ground level in this case) is a zero flux boundary condition such that pollutants are not fed into the model through the top boundary. [b] Used in a diagnostic model simulation to investigate the effects of increasing the boundary condition values to match those used by the South Coast Air Quality Management District (*51*). [c] Non-methane hydrocarbon (NMHC) concentrations are specified in ppb C instead of ppbv. Each ppb C of NMHC is speciated as follows: 0.095 ppbv ALKA, 0.017 ppbv ETHE, 0.018 ppbv ALKE, 0.015 ppbv TOLU, and 0.016 ppbv AROM.

4. *Model Results*

In the sections above, the CIT model formulation and input data setup procedures have been described. In this section, the model results obtained using the CIT airshed model are presented for the August 27–29, 1987, episode. Model results are presented for ozone and for key ozone precursors including nitrogen dioxide and reactive hydrocarbons. It is important to consider model performance for ozone precursors in addition to ozone itself to improve confidence in apparent agreement between observed and predicted ozone concentrations. While results are given for all 3 days, the discussion presented here will focus on predictions for August 28. That is because results on the first day of the calculations (August 27) are sensitive to the choice of initial conditions, and because those for August 29 (a Saturday) are uncertain due to the lack of a mobile source emission inventory that reflects traffic patterns appropriate for Friday evening and Saturday.

The spatial distribution of ground-level 1-h average ozone concentrations at the time of the observed ozone peak (1400–1500 h PST on August 28) is presented in Figure 2 for the base case calculation. Inspection of Figure 2 shows that the model predicts that a substantial fraction of the eastern portion of the South Coast Air Basin exceeds the 12 pphm National Ambient Air Quality Standard. Peak ozone predictions are generally lower than observed concentrations. Ozone predictions obtained using in-

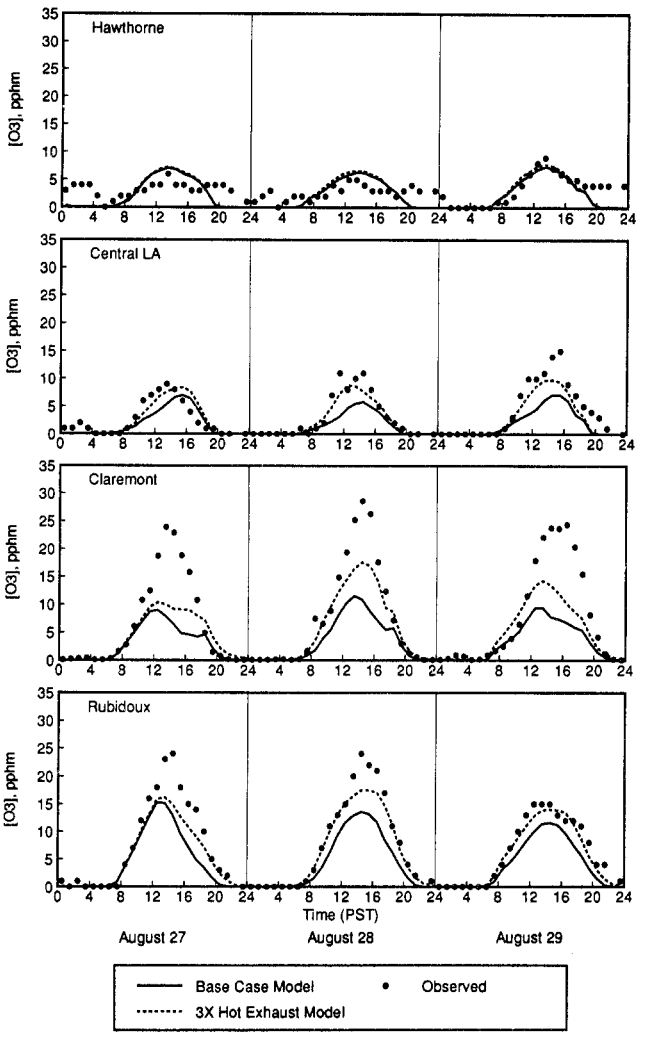

Figure 4. Time series plots of observed ozone concentrations (solid circles) and model predictions for the base case (solid line) and for the case of increased on-road vehicle hot exhaust emissions (dashed line).

creased organic gas exhaust emissions are presented in Figure 3. In this case generally higher ozone concentrations are predicted. The region of high ozone concentrations is shifted westward toward the source-rich coastal and central regions of the air basin.

Time series plots showing diurnal patterns of ozone concentrations over the entire 3-day episode are shown in Figure 4. The monitoring stations selected for inclusion in Figure 4 were all intensive monitoring sites during SCAQS and define a cross section taken across the center of the air basin starting at the coast with Hawthorne and proceeding inland to Rubidoux. Using the official emission inventory, the model reproduces the temporal behavior seen in the observed data, but tends to underpredict peak ozone concentrations at the inland sites. The 34% increase in organic gas emissions represented by the increased exhaust emission perturbation discussed earlier brings the model into closer agreement with observed ozone levels, especially at sites such as Glendora where observed ozone concentrations were highest and underpredictions in the base case calculation were largest. A statistical comparison of observations and model predictions is presented in Table V. Note that ozone concentration data from 37 air monitoring sites located within the modeling region were used in the statistical comparison, while only a few representative sites are shown in Figure 4.

In order to assess model performance for ozone, one must also consider the ability of the model to predict the

Table V. Analysis of Model Performance for Ozone on August 28

statistical measure[a]	base case model[b]	3× hot exhaust model[c]	typical performance[d]
bias (pphm)	−3.2	−0.4	
normalized bias (%)	−23	+1	±15
σ of residuals (pphm)	4.6	3.9	
gross error (pphm)	4.3	3.0	
normalized gross error (%)	38	29	35
peak prediction accuracy			
average station, $\bar{A}$ (%)	−26	−7	
basinwide maximum, A_u (%)	−54	−33	±20

[a] Tesche et al. (*51*). The statistical measures are calculated using all pairs of predicted and observed concentrations where the observed value is greater than or equal to the cutoff of 6 pphm. The bias is defined as the mean residual (predicted − observed) concentration, and the normalized bias is computed by dividing each residual by the corresponding observed concentration and then averaging as for the bias. The gross error statistics are computed in the same manner as the bias statistics, except that the absolute values of the residuals are used throughout. The peak prediction accuracy statistics are calculated using only the peak 1-h observed concentrations. The average station peak prediction accuracy ($\bar{A}$) compares peak observed values with peak predicted values at the same location but not necessarily paired in time. The basinwide peak accuracy (A_u) focuses on the single site with the highest observed concentration and compares this value with the peak model prediction within a radius of 25 km over a time interval extending from 3 h before until 3 h after the time of the observed peak. [b] From the CIT airshed model using the baseline emission inventory. [c] From the CIT airshed model using scaled-up on-road vehicle hot exhaust emissions. [d] Technical guidance for "typical" ozone model performance (*52*).

Table VI. Analysis of Model Performance for Ozone Precursors on August 28

statistical measure[a]	base case model[b]	3× hot exhaust model[c]
total NO_2[d]		
bias (pphm)	+0.1	+0.4
normalized bias (%)	+17	+22
σ of residuals (pphm)	2.3	2.4
gross error (pphm)	1.8	1.8
normalized gross error (%)	41	44
reactive hydrocarbons		
bias (ppbv)	−56	−29
normalized bias (%)	−35	−12
σ of residuals (ppbv)	62	68
gross error (ppbv)	71	59
normalized gross error (%)	51	47

[a] Tesche et al. (*51*). The definitions of the statistical measures are presented in the footnotes to Table V. A cutoff value of 2 pphm was used for NO_2; no cutoff was used for reactive hydrocarbons. [b] From the CIT airshed model using the baseline emission inventory. [c] From the CIT airshed model using scaled-up on-road vehicle hot exhaust emissions. [d] Total NO_2 includes NO_2 plus all other reactive nitrogen compounds that are measured as if they were NO_2 by chemiluminescent monitors.

concentrations of key ozone precursors. In Figure 5, comparisons between observed and predicted NO_2 concentrations are presented. The statistical analysis for NO_2 shown in Table VI is based on all available air monitoring data (26 sites). The response of chemiluminescent NO_x monitors to species other than NO and NO_2 has been studied by Winer et al. (*49*). It is known that such instruments, when operating in NO_x mode, respond to both NO_2 and other nitrogen-containing species including nitric acid and peroxyacetyl nitrate. For this reason, the model predictions for NO_2 and other reactive nitrogen compounds that are measured as if they were NO_2 were summed to

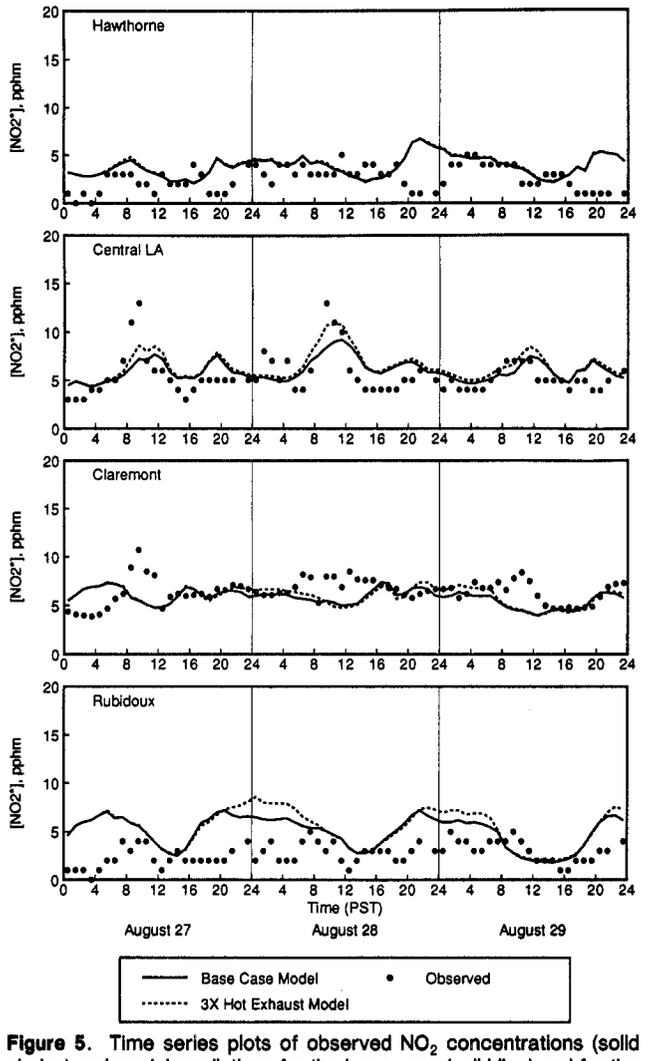

Figure 5. Time series plots of observed NO_2 concentrations (solid circles) and model predictions for the base case (solid line) and for the case of increased on-road vehicle hot exhaust emissions (dashed line).

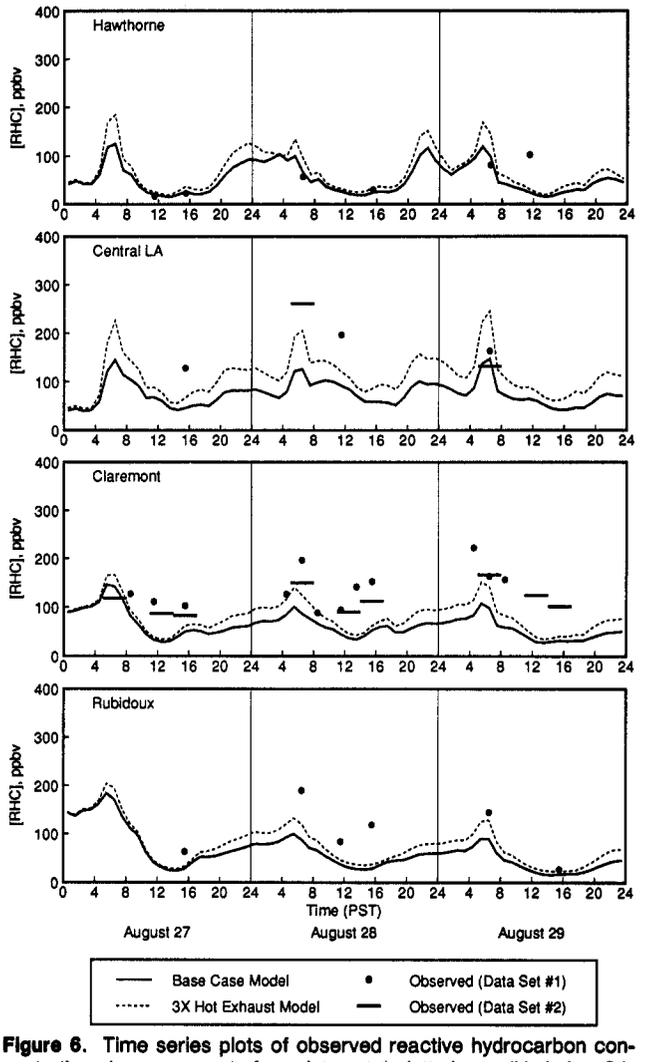

Figure 6. Time series plots of observed reactive hydrocarbon concentrations (measurements from data set 1 plotted as solid circles; 3-h average samples from data set 2 plotted as horizontal bars) and model predictions for the base case (solid line) and for the case of increased on-road vehicle hot exhaust emissions (dashed line).

give "total" NO_2 predictions for comparison with observed NO_2 concentrations.

Figure 6 shows similar comparisons for the reactive hydrocarbons. Methane, ethane, and acetylene were excluded from this comparison because they are treated as unreactive compounds in the LCC chemical mechanism. The oxygenated species such as aldehydes, alcohols, and glycols were lumped separately from the hydrocarbons and have been excluded from this comparison because the database of measured concentrations does not include all of the relevant oxygenated species. As shown in Figure 6, there were two sets of special hydrocarbon concentration measurements made during SCAQS. The first set of measurements (data set 1) was made by Stockburger et al. (*47*). A second independent set of measurements (data set 2) was made by Lonneman et al. (*50*). The statistical comparison of predicted and observed reactive hydrocarbon concentrations shown in Table VI is based on data set 1, which includes multiple concentration measurements each day at all of the eight intensive monitoring sites located within the modeling region (see Figure 1). The samples in data set 2 were collected over 3-h intervals with three samples per day at Claremont, and one additional early morning sample collected each day at both the Central Los Angeles and Long Beach City College sites. As shown in Table VI, ambient hydrocarbon concentrations are underpredicted when the official emission inventory is used in the base case calculation. The perturbation involving increased on-road vehicle exhaust emissions bring hydrocarbon predictions closer to observed levels.

It should be noted that the case of increased hot exhaust emissions considered here does not represent a complete correction of all possible biases in the emission inventory. The purpose of this analysis was only to examine the effects of increasing on-road vehicle hot exhaust emissions to match emission rates measured in the Van Nuys tunnel (*11*, *12*). Organic gas emissions from other sources could also be understated in the official emission inventory. Further increases in organic gas emissions to the model (beyond the increase in hot exhaust emissions already considered) lead to higher predicted ozone concentrations and better agreement with observed hydrocarbon concentrations.

5. *Sensitivity Analysis*

As part of any detailed assessment of airshed model performance, a set of diagnostic simulations are recommended (*51*). A series of such simulations has been conducted using the CIT airshed model, as described below.

In the first simulation, the model was run using the increased boundary conditions shown in Table IV. These values are comparable to those used by the South Coast Air Quality Management District in their modeling of air

quality in the Los Angeles area over the same intensive modeling period (*48*). The CIT airshed model predicts higher ozone concentrations (higher by 3–7 pphm) generally closer to the observed values, when the increased boundary conditions are used. There is, however, little evidence in the SCAQS database supporting the use of such high boundary conditions.

Further diagnostic simulations using very clean boundary conditions and initial conditions showed that the base case model predictions described in the previous section were not driven by the boundary conditions and that model predictions were sensitive to the choice of initial conditions only on the first day of simulation. Use of clean boundary conditions led to model predictions that were virtually identical to those calculated in the base case.

Model sensitivity to dry deposition was examined in a calculation where the deposition of all pollutants was eliminated. Predicted ozone concentrations increased throughout the basin, by about 1 pphm at sites near the coast, and by 2–4 pphm at inland sites. The largest increases were seen at sites located farthest downwind. In another simulation, the surface resistance terms for deposition of ozone and hydrogen peroxide were decreased by factors of 2 and 10, respectively. The dry deposition flux of these pollutants was thereby increased, though not in proportion to the change in surface resistance values since mass transport considerations provide an upper limit to the dry deposition flux. Predicted ozone concentrations decreased slightly (by 0–2 pphm) following the changes in surface resistance values.

The sensitivity of model predictions to changes in meteorological variables also has been considered. When all wind speeds were reduced by 50% in the model, predicted ozone concentrations at inland sites increased by up to 5 pphm, especially from 1200 to 1600 h PST, when the sea breeze was strongest. Doubling the mixed-layer depth in the model resulted in slight increases in predicted ozone concentrations, whereas predicted carbon monoxide concentrations decreased. When the ground-level photolysis rate scaling factors were removed, and only model-predicted clear sky photolysis rate constants were used as per eq 7, predicted ozone concentrations increased by 1–3 pphm. The largest increases were seen near the Rubidoux monitoring site, where the base case photolysis scaling factor was lowest.

Predicted ozone concentrations did not increase significantly when the biogenic hydrocarbon emissions to the model were increased to 3 times the baseline values. This is not surprising given that the emission inventory specifies that the biogenic emissions occur mainly in forested areas in the mountains away from and generally downwind of the urbanized portions of the basin (*35*).

Finally, a series of diagnostic simulations involving removal of pollutant emissions were performed. The zeroing of NO_x emissions led to virtually background air quality by the second day of the simulation. Similar results were obtained when all pollutant emissions were removed from the model. A simulation with zero organic gas emissions resulted in very low predicted ozone concentrations due to NO_x scavenging of background ozone.

6. Discussion

The possibility that the official Los Angeles organic gas emission inventory is understated has been discussed in several recent studies (*1*, *11–13*). Results from the present study further suggest that organic gas emissions are in fact understated. The sensitivity of ozone predictions to increased organic gas emissions is greatest at sites showing the largest ozone concentration underpredictions in the base case simulation. The response shown in Figure 4 at Claremont to a 34% increase in overall organic gas emissions (the hot exhaust perturbation) is typical of other nearby sites where the peak observed ozone concentrations were underpredicted in the base case simulation. In Figure 5, the time series plots for total NO_2 (which includes NO_2 plus other reactive nitrogen compounds that were measured as if they were NO_2) show that the model is carrying approximately the correct total amount of reactive nitrogen compounds.

Nighttime concentrations of NO_x and hydrocarbons are generally overpredicted at coastal sites such as Long Beach. Examination of nighttime upper air soundings for August 27–29 at Long Beach indicates that the low observed concentrations of primary pollutants result from significant vertical mixing that is not fully reproduced by the model. The upper air soundings show that the nocturnal boundary layer at Long Beach is neutrally stratified, while the model assumes slightly stable conditions. Another possible explanation is that the emission inventory may specify unrealistic levels of nighttime source activity in these areas.

In the present study, model simulations using increased on-road vehicle organic gas and carbon monoxide hot exhaust emissions were performed (in addition to simulations using the baseline emission inventory) in order to approximate the actual motor vehicle emissions as observed in recent roadway tunnel measurements. Use of this scaled-up inventory resulted in higher predicted ozone concentrations that were closer to observed values, with increases of up to 8 pphm seen at some sites. Reactive hydrocarbon concentrations were still underpredicted (−12% on average) even after the increase in on-road vehicle hot exhaust emissions. Thus, there may be additional organic gas emissions missing from the offiical inventory, beyond those accounted for by scaling up the mobile source hot exhaust emissions.

7. Conclusions

The CIT airshed model has been improved and updated using a new chemical mechanism (*14*) and a new dry deposition module (*9*). Documentation in the form of a user's guide has been prepared (*16–18*).

The CIT model has been applied to the South Coast Air Basin during the August 27–29, 1987, SCAQS intensive monitoring period. In the base case simulation, using the official emission inventory, peak ozone concentrations were substantially underpredicted. When an alternate emission inventory with increased organic gas and carbon monoxide hot exhaust emissions was used to reflect recent measurements of on-road motor vehicle exhaust emissions, the CIT model predicted higher ozone and hydrocarbon concentrations that matched the observed data more closely.

Acknowledgments

We gratefully acknowledge the assistance of Bart Croes and Paul Allen of the California Air Resources Board in supplying SCAQS-related data. We also thank Dr. Julia Lester of the South Coast Air Quality Management District for providing biogenic emission data. We thank all of the CRC reviewers for their numerous helpful comments.

Literature Cited

(1) National Research Council. *Rethinking the ozone problem in urban and regional air pollution*; National Academy Press: Washington, DC, 1991.
(2) Seinfeld, J. H. *J. Air Pollut. Control Assoc.* **1988**, *38*, 616–645.

(3) McRae, G. J.; Goodin, W. R.; Seinfeld, J. H. *Atmos. Environ.* **1982**, *16*, 679–696.
(4) McRae, G. J.; Goodin, W. R.; Seinfeld, J. H. *Atmos. Environ.* **1983**, *17*, 501–522.
(5) Russell, A. G.; McCue, K. F.; Cass, G. R. *Environ. Sci. Technol.* **1988**, *22*, 263–271.
(6) Russell, A. G.; McCue, K. F.; Cass, G. R. *Environ. Sci. Technol.* **1988**, *22*, 1336–1347.
(7) Milford, J. B.; Russell, A. G.; McRae, G. J. *Environ. Sci. Technol.* **1989**, *23*, 1290–1301.
(8) Russell, A. G.; St. Pierre, D.; Milford, J. B. *Science* **1990**, *247*, 201–205.
(9) Russell, A. G.; Winner, D. A.; McCue, K. F.; Cass, G. R. Mathematical modeling and control of the dry deposition flux of nitrogen-containing air pollutants. Report to the California Air Resources Board under Contract A6-188-32. EQL Report 29, Environmental Quality Laboratory, California Institute of Technology, Pasadena, CA, 1992.
(10) Lawson, D. R. *J. Air Waste Manage. Assoc.* **1990**, *40*, 156–165.
(11) Ingalls, M. N.; Smith, L. R.; Kirksey, R. E. Measurement of on-road vehicle emission factors in the California South Coast Air Basin. Volume I: regulated emissions. Report to the Coordinating Research Council under Project SCAQS-1. Southwest Research Institute, San Antonio, TX, 1989.
(12) Pierson, W. R.; Gertler, A. W.; Bradow, R. L. *J. Air Waste Manage. Assoc.* **1990**, *40*, 1495–1504.
(13) Fujita, E. M.; Croes, B. E.; Bennett, C. L.; Lawson, D. R.; Lurmann, F. W.; Main, H. H. *J. Air Waste Manage. Assoc.* **1992**, *42*, 264–276.
(14) Lurmann, F. W.; Carter, W. P. L.; Coyner, L. A. A surrogate species chemical reaction mechanism for urban-scale air quality simulation models. Volumes I and II. Report to the U.S. Environmental Protection Agency under Contract 68-02-4104. ERT Inc., Newbury Park, CA, and Statewide Air Pollution Research Center, University of California, Riverside, CA, 1987.
(15) Harley, R. A.; Russell, A. G.; McRae, G. J.; McNair, L. A.; Winner, D. A.; Odman, M. T.; Dabdub, D.; Cass, G. R.; Seinfeld, J. H. Continued development of a photochemical model and application to the Southern California Air Quality Study (SCAQS) intensive monitoring periods: Phase I. Report to the Coordinating Research Council under Project SCAQS-8. Carnegie Mellon University, Pittsburgh, PA, and California Institute of Technology, Pasadena, CA, 1992.
(16) McRae, G. J.; Russell, A. G.; Harley, R. A. CIT photochemical airshed model—installation and operation manual. Report to the Coordinating Research Council under Project SCAQS-8. Carnegie Mellon University, Pittsburgh, PA, and California Institute of Technology, Pasadena, CA, 1992.
(17) McRae, G. J.; Russell, A. G.; Harley, R. A. CIT photochemical airshed model—data preparation manual. Report to the Coordinating Research Council under Project SCAQS-8. Carnegie Mellon University, Pittsburgh, PA, and California Institute of Technology, Pasadena, CA, 1992.
(18) McRae, G. J.; Russell, A. G.; Harley, R. A. CIT photochemical airshed model—systems manual. Report to the Coordinating Research Council under Project SCAQS-8. Carnegie Mellon University, Pittsburgh, PA, and California Institute of Technology, Pasadena, CA, 1992.
(19) Carter, W. P. L. *Atmos. Environ.* **1990**, *24A*, 481–518.
(20) Japar, S. M.; Wallington, T. J.; Richert, J. F. O.; Ball, J. C. *Int. J. Chem. Kinet.* **1990**, *22*, 1257–1269.
(21) Atkinson, R. *Atmos. Environ.* **1990**, *24A*, 1–41.
(22) Russell, A. G.; McRae, G. J.; Cass, G. R. *Atmos. Environ.* **1983**, *17*, 949–964.
(23) Russell, A. G.; Cass, G. R. *Atmos. Environ.* **1986**, *20*, 2011–2025.
(24) Businger, J. A.; Wyngaard, J. C.; Izumi, Y.; Bradley, E. F. *J. Atmos. Sci.* **1971**, *28*, 181–189.
(25) Sheih, C. M.; Wesely, M. L.; Walcek, C. J. A dry deposition module for regional acid deposition. EPA-600/3-86-037; Atmospheric sciences laboratory, U.S. Environmental Protection Agency, Research Triangle Park, NC, 1986.
(26) Peterson, J. T. Calculated actinic fluxes (290–700 nm) for air pollution photochemistry applications. EPA-600/4-76-025; U.S. Environmental Protection Agency, Research Triangle Park, NC, 1976.
(27) Zafonte, L.; Rieger, P. L.; Holmes, J. R. *Environ. Sci. Technol.* **1977**, *11*, 483–487.
(28) Madronich, S. *Atmos. Environ.* **1987**, *21*, 569–578.
(29) Holtslag, A. A. M.; Ulden, A. P. V. *J. Clim. Appl. Meteorol.* **1983**, *22*, 517–529.
(30) Mirabella, V.; Nazemi, M. Development of the SCAQS emission inventory: an overview. Presented at the 82nd annual meeting of the Air & Waste Management Association, Anaheim, CA, 1989; Paper 89-111.4.
(31) Wagner, K. K.; Allen, P. D. SCAQS emissions inventory for August 27–29, 1987 (Tape ARA714). Technical Support Division, California Air Resources Board, Sacramento, CA, personal communication, 1990.
(32) Yotter, E. E.; Wade, D. L. Development of a gridded motor vehicle emission inventory for the Southern California Air Quality Study. Presented at the 82nd annual meeting of the Air & Waste Management Association, Anaheim, CA, 1989; Paper 89-137.2.
(33) Winer, A. M. Investigation of the role of natural hydrocarbons in photochemical smog formation in California. Report to the California Air Resources Board under Contract A0-056-32. Statewide Air Pollution Research Center, Riverside, CA, 1983.
(34) Winer, A. M.; Arey, J.; Aschmann, S. M.; Atkinson, R.; Long, W. D.; Morrison, L. C.; Olszyk, D. M. Hydrocarbon emissions from vegetation found in California's Central Valley. Report to the California Air Resources Board under Contract A732-155. Statewide Air Pollution Research Center, University of California, Riverside, CA, 1989.
(35) Horie, Y.; Sidawi, S.; Ellefsen, R. Inventory of leaf biomass and emission factors for vegetation in the South Coast Air Basin. Report to the South Coast Air Quality Management District under Contract 90163. Valley Research Inc., Van Nuys, CA, 1990.
(36) Causley, M. C.; Wilson, G. M. Seasonal and annual average biogenic emissions for the South Coast Air Basin generated by the SCAQMD biogenic data base system. Report to the South Coast Air Quality Management District under Contract 90177. Systems Applications International, San Rafael, CA, 1991.
(37) Gharib, S.; Cass, G. R. Ammonia emissions in the South Coast Air Basin. Open file report 84-2. Environmental Quality Laboratory, California Institute of Technology, Pasadena, CA, 1984.
(38) Dickson, R. J.; Oliver, W. R. Approach to developing the SCAQS high-resolution ammonia emission inventory. Presented at the 82nd annual meeting of the Air & Waste Management Association, Anaheim, CA, 1989; Paper 89-137.6.
(39) Croes, B. E. Research Division, California Air Resources Board, Sacramento, CA, personal communication, 1990.
(40) Goodin, W. R.; McRae, G. J.; Seinfeld, J. H. *J. Appl. Meteorol.* **1979**, *18*, 761–771.
(41) Goodin, W. R.; McRae, G. J.; Seinfeld, J. H. *J. Appl. Meteorol.* **1980**, *19*, 98–108.
(42) Lehrman, D.; Knuth, W.; Alexander, N.; Giroux, H.; Lehrman, L. SCAQS meteorological support program. Report to the California Air Resources Board under Contract A6-097-32. Technical & Business Systems, Santa Rosa, CA, 1988.
(43) Hanna, S. R.; Chang, J. C. *Boundary Layer Meteorol.* **1992**, *58*, 229–259.
(44) McRae, G. J. *J. Air Pollut. Control Assoc.* **1980**, *30*, 394–396.
(45) Anderson, J. A.; Koos, J. C.; Hammarstrand, R. G. M. Summary of SCAQS upper air measurements performed by the STI aircraft. Report to the California Air Resources Board under Contract A6-098-32. Sonoma Technology Inc., Santa Rosa, CA, 1989.
(46) Main, H. H.; Lurmann, F. W.; Roberts, P. T. Pollutant concentrations along the western boundary of the South Coast Air Basin. Part I: a review of existing data. Report to the South Coast Air Quality Management District.

Sonoma Technology, Inc., Santa Rosa, CA, 1990.
(47) Stockburger, L.; Knapp, K. T.; Ellestad, T. G. Overview and analysis of hydrocarbon samples during the summer Southern California Air Quality Study. Presented at the 82nd annual meeting of the Air & Waste Management Association, Anaheim, CA, 1989; Paper 89-139.1.
(48) Ozone modeling—performance evaluation. Draft Technical Report V-B, Air Quality Management Plan, 1991 Revision. South Coast Air Quality Management District, El Monte, CA, 1990.
(49) Winer, A. M.; Peters, J. W.; Smith, J. P.; Pitts, J. N. *Environ. Sci. Technol.* **1974**, *8*, 1118-1121.
(50) Lonneman, W. A.; Seila, R. L.; Ellenson, W. Speciated hydrocarbon and NO_x comparisons at SCAQS source and receptor sites. Presented at the 82nd annual meeting of the Air & Waste Management Association, Anaheim, CA, 1989; Paper 89-152.5.
(51) Tesche, T. W.; Georgopoulos, P.; Seinfeld, J. H.; Cass, G. R.; Lurmann, F. W.; Roth, P. M. Improvement of procedures for evaluating photochemical models. Report to the California Air Resources Board under Contract A832-103. Radian Corp., Sacramento, CA, 1990.
(52) DaMassa, J. Technical guidance document: photochemical modeling. Technical Support Division, California Air Resources Board, Sacramento, CA, 1992.

Received for review June 1, 1992. Revised manuscript received October 15, 1992. Accepted October 26, 1992. This study was sponsored by the Coordinating Research Council (CRC) under Project SCAQS-8.

Monitoring of Malathion and Its Impurities and Environmental Transformation Products on Surfaces and in Air Following an Aerial Application

Mark A. Brown,* Myrto X. Petreas, Howard S. Okamoto, Thomas M. Mischke, and Robert D. Stephens

California Department of Health Services, Hazardous Materials Laboratory, Berkeley, California 94704

■ Concentrations in air and on surfaces of malathion and impurities [malaoxon, isomalathion, *O,O,S*-trimethyl phosphorodithioate, *O,O,O*-trimethyl phosphorothioate, *O,O,S*-trimethyl phosphorothioate, and diethyl fumarate (DEF)] were determined at three sites during and for 9 days after a 1990 aerial spraying in California. Malathion spray was transformed via oxidation to malaoxon, hydrolysis to DEF, and selective volatilization. Malathion half-lives were 1.6 to >9 days, and depositions at three sites ranged from 1100 to 2413 $\mu g/ft^2$, while malaoxon ranged from 2.9 to 6.0 $\mu g/ft^2$. Malaoxon increased fastest on filter paper surfaces, e.g., initial deposition of 7 $\mu g/ft^2$ increasing to 315 $\mu g/ft^2$ after 9 days. Malathion air concentrations increased to 80 ng/m^3 within 1 day, and malaoxon to 64 ng/m^3 at 24-48 h: Both were detectable after 9 days. DEF surface levels increased over 9 days; air concentrations persisted for 72 h. The three phosphoro(di)thioate trimethyl esters were undetectable on surfaces within 24 h, producing an air burst apparently via rapid volatilization. Accurate human exposure assessment during malathion spraying must consider environmental transformations.

Introduction

In 1989 and 1990 the California Department of Food and Agriculture (CDFA) conducted aerial applications of a malathion/protein bait mixture in urban areas of southern California in an effort to eradicate an outbreak of the Mediterranean fruit fly. Human exposure to malathion and malathion-related impurities was estimated by assuming that relative concentrations of these compounds measured in the spray mixture did not change after aerial application. During these applications, CDFA monitored the deposition of malathion and malaoxon on a single type of surface and concentrations in air for a maximum of 48 h. The California Department of Health Services (CDHS) initiated a parallel study during a single spray episode in May 1990 to monitor malathion and six impurities with known mammalian toxicities, on three different surface types and in air over a 10-day time period. The study was designed to estimate amounts and variations in the concentrations of malathion and its impurities in the technical grade malathion concentrate and in the concentrate/bait formulated tank mixture and the environmental fate of malathion and related impurities present initially in the spray mixture, and after deposition on three types of surfaces, and in air for a period of 9 days following aerial application.

The malathion-related impurities measured in this study were selected on the basis of information about their relative acute and chronic toxicities. Unfortunately, most available data come from animal studies and far less information is available about human toxicities for these compounds.

Acute Toxicity of Malathion and Related Impurities. Malathion, introduced in 1950 by American Cyanamid Co., is a nonsystemic organophosphorus insecticide (*1*). Its low acute mammalian toxicity is due to its selective hydrolytic degradation, via mammalian carboxylesterases, versus its oxidative activation to the potent acetylcholinesterase inhibitor malaoxon in insects. Manufacture of malathion results in production of various impurities (Table I). The structures and abbreviations of some of the most toxicologically relevant malathion impurities are shown in Figure 1.

The increased and highly variable rat oral toxicity of technical versus highly purified malathion correlates specifically to concentrations of the impurity isomalathion (*2*). A direct correlation was shown between the inhibition of mouse serum or liver malathion carboxylesterase activity and LD_{50}'s to rats and mice treated with technical malathion (*3*). The malathion impurities isomalathion, OSS(O), OOS(O), and OOS(S) increase malathion acute rat oral toxicity and act as effective inhibitors of rat liver carboxylesterases that are involved in the hydrolytic detoxification of malathion (*4*). Small amounts of these impurities significantly increase the rat acute oral toxicity of technical malathion; e.g., 1% isomalathion or OSS(O) increases malathion toxicity 6- or 12-fold, respectively (*2*). Isomalathion and related *O,O*-dimethyl phosphoro(di)thioate ester impurities are significantly more potent inhibitors of mammalian acetylcholine esterases than malathion, with bimolecular inhibition constants (k_{is}) approximately 1000 times greater than malathion (*5*).

In contrast to the rat, only isomalathion is effective in inhibiting human liver carboxylesterase at concentrations

* Current address: Congress of the United States, Office of Technology Assessment, 600 Pennsylvania Ave. S.E., Washington, DC, 20003.

 0013-936X/93/0927-0388$04.00/0